

Using ~170 MgII Absorbers to Understand Galactic Winds and IGM Accretion



Nikole M. Nielsen¹, Chris W. Churchill¹, Glenn G. Kacprzak²

¹New Mexico State University, ²Swinburne University of Technology



Introduction & Motivation

Inflowing and outflowing gas in galaxy halos is important in star formation. Background quasar (QSO) spectra provide sensitive absorption lines from these gaseous halos. The MgII $\lambda\lambda 2796, 2803$ doublet is ideal since it samples galaxies over the redshift range where the galaxies can be studied in detail. MgII is observed in outflowing winds (e.g., Weiner et al. 2009) and in infalling accretion (e.g., Rubin et al. 2012). Other studies have reported trends between MgII absorption and star formation rate, B-band luminosity, and/or stellar mass of the host galaxy (e.g., Chen et al. 2010; Ménard et al. 2011). Recent works indicate that the gas is preferentially located along the minor axis or the major axis of the host galaxy (e.g., Kacprzak et al. 2012), suggesting bipolar outflowing winds and coplanar accretion are the dominant structures traced by MgII absorption.

As such, increasing the sample size of known MgII absorbers and their host galaxies holds the promise of furthering our understanding of gas flows in galaxies. Many previous surveys have been published with samples no larger than ~80 galaxies. In many cases, magnitudes, colors, and QSO-galaxy projected separations are not directly comparable between samples due to differing cosmologies and magnitude systems. It is desirable to standardize previous surveys to form a large uniform sample of MgII absorption-selected galaxies.

Data Collection & Method

We built a catalog of 169 isolated MgII absorption-selected galaxies (median $z = 0.35$) taken from our work and a literature search. We standardized all galaxy impact parameters and photometric properties to the current Λ CDM cosmology and placed all B- and K-band absolute magnitudes on the AB system using uniform k -corrections (see Kim et al. 1996) of the SEDs of Mannucci et al. (2001). B-K or B-R rest-frame colors were calculated from absolute magnitudes or transposed using the linear relation: $(B-K) = 2.05(B-R) - 0.25$.

We applied halo abundance matching using the Bolshoi cosmological simulations (Trujillo-Gomez et al. 2011) to obtain galaxy virial masses, M_{vir} , from absolute r magnitudes. We computed virial radii, R_{vir} , from the formalism of Bryan & Norman (1998).

Sample

We present our standardized galaxy sample in Figures 1 and 2. In Figure 1, impact parameter (D) is plotted against galaxy redshift (z_{gal}). Point colors represent different $W_r(2796)$ bins (see legend). Figure 2 presents three dimensional distributions of QSO-galaxy D , galaxy B-band luminosity (L_B), and absolute K magnitude (M_K). Galaxy types were assigned based on the following color cuts:

Early	$(B-K) \geq 1.76$
Late	$1.16 < (B-K) < 1.76$
Irregular	$(B-K) \leq 1.16$

Figure 1: z vs D

Colored points indicate different $W_r(2796)$ bins (see legend). Open points represent galaxies which have limits for $W_r(2796)$.

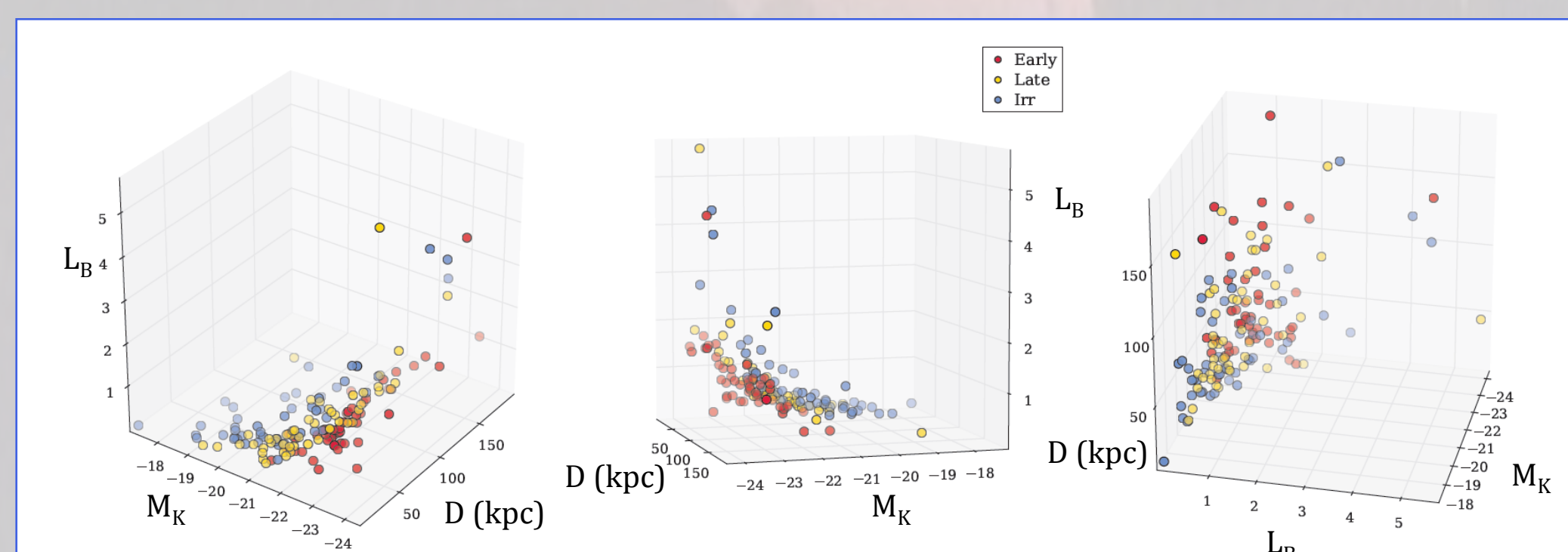
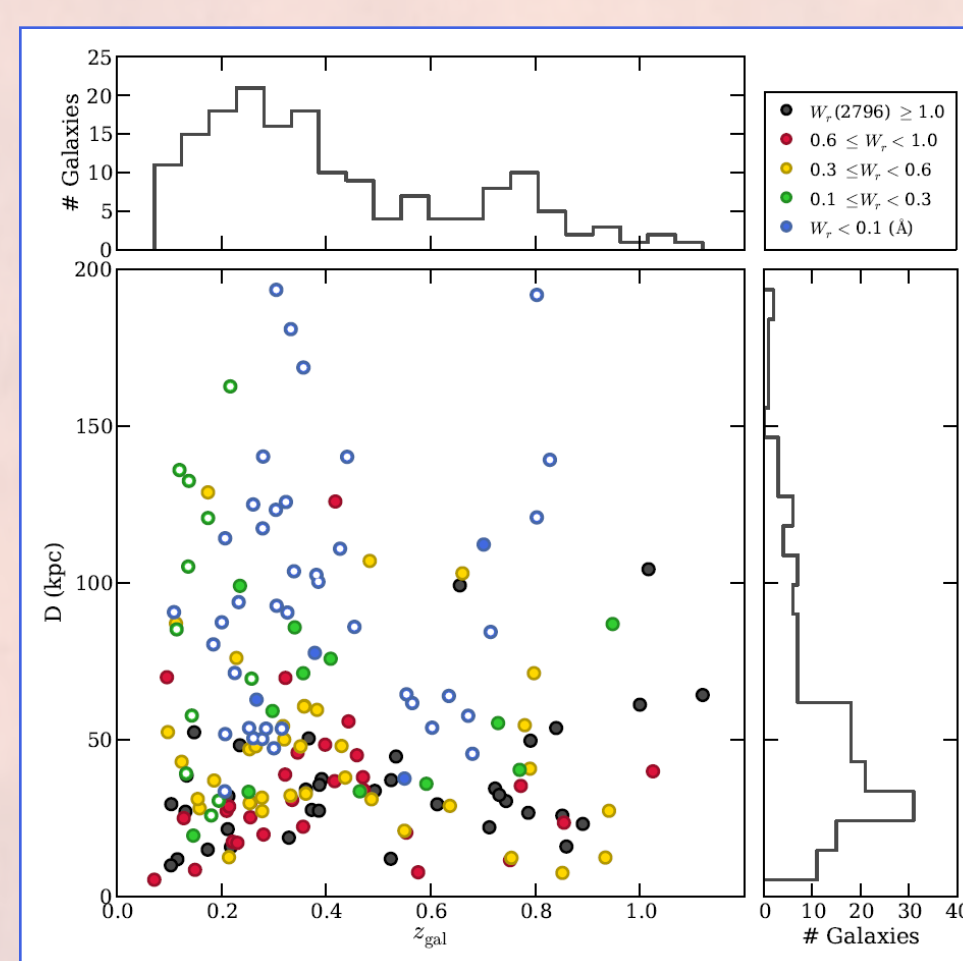


Figure 2: L_B vs M_K vs D

The sample is shown in three different orientations for L_B vs M_K vs D . Data points are color coded by galaxy type (see legend). Only galaxies with measured colors are plotted.

$W_r(2796)$ & Impact Parameter

In Figure 3, we plot $W_r(2796)$ against D . $W_r(2796)$ is anti-correlated with D at the 8.2σ level (accounting for limits), indicating that the quantity of halo gas diminishes with projected distance. A log-linear fit, $\log W_r(2796) = \alpha_1 D + \alpha_2$, is the best parameterization of the data, with $\alpha_1 = -0.019 \pm 0.002$ and $\alpha_2 = 0.28 \pm 0.11$. The considerable scatter about this relation suggests that $W_r(2796)$ is governed by physical processes related to the galaxy such as luminosity, star formation, or orientation.

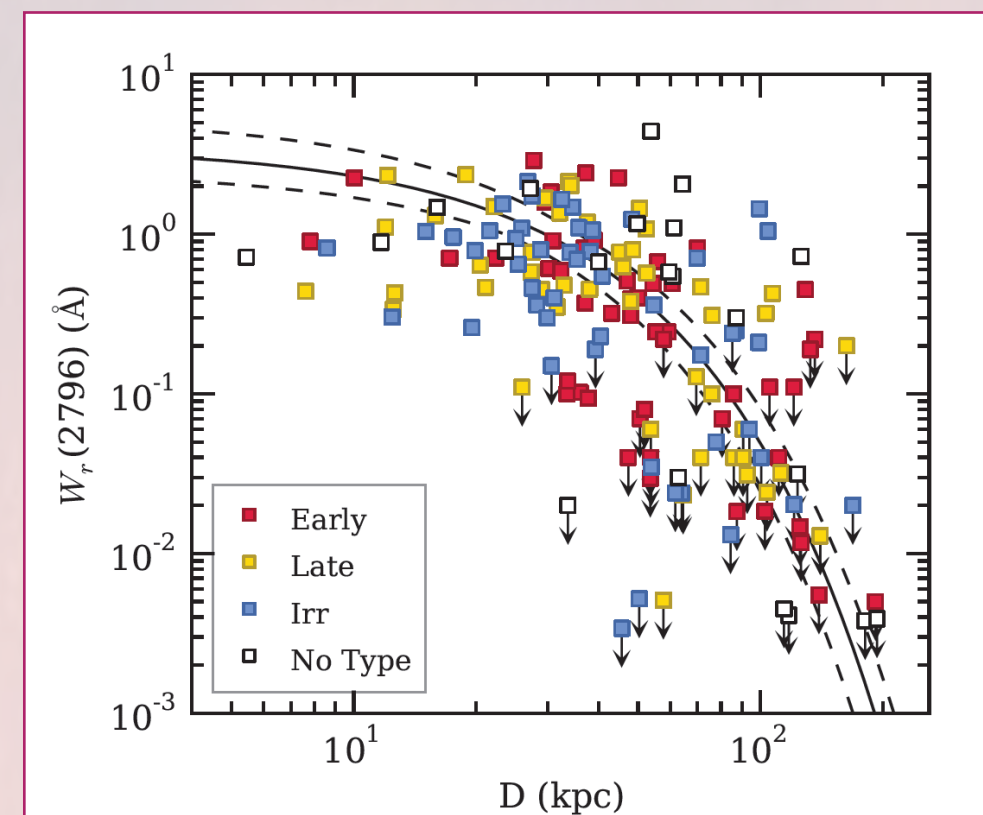


Figure 3: $W_r(2796)$ vs D

The solid line is a log-linear maximum likelihood fit to the data and the dashed curves provide 1σ uncertainties.

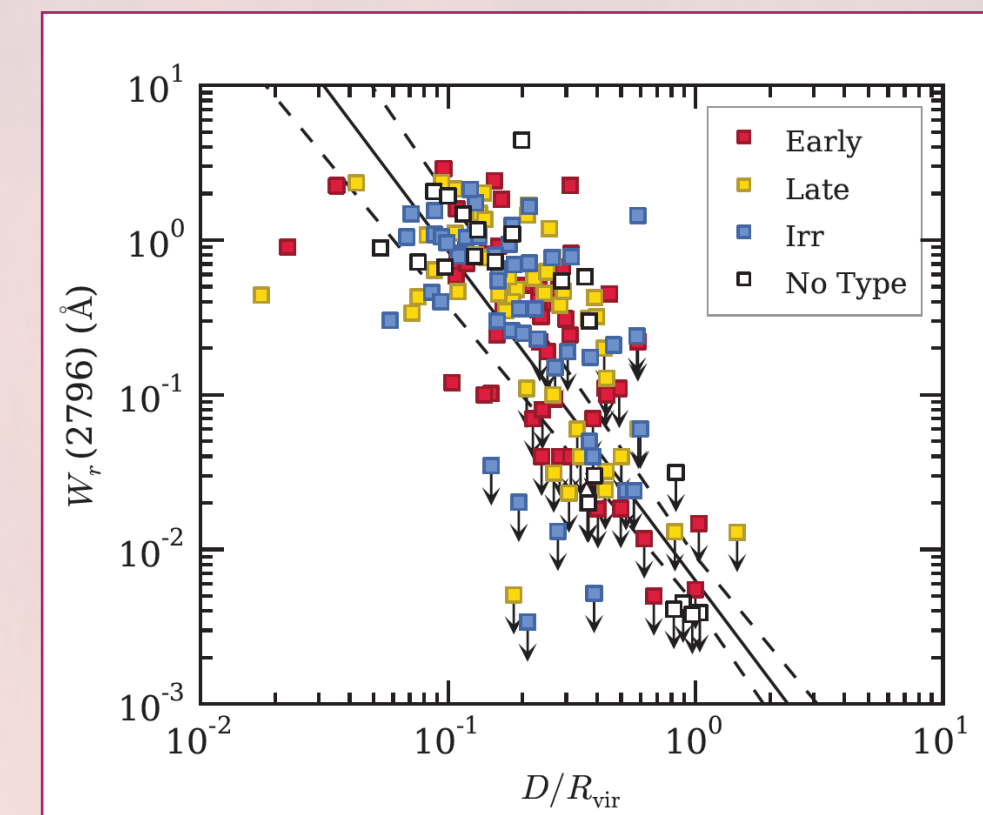


Figure 4: $W_r(2796)$ vs D/R_{vir}

The solid line is a log-log maximum likelihood fit to the data and the dashed curves provide 1σ uncertainties.

$W_r(2796)$ Dependence with Virial Radius

In Figure 4, we plot $W_r(2796)$ against D/R_{vir} , which ranges from ~0.1 to ~1. A tight anti-correlation appears with a 9.4σ level. A log-log fit, $\log W_r(2796) = \alpha_1 \log D + \alpha_2$ is the best parameterization of the data, with $\alpha_1 = -2.13 \pm 0.19$ and $\alpha_2 = -2.20 \pm 0.16$. This reveals an inverse square dependence of $W_r(2796)$ with the projected distance from the galaxy relative to the extent of its virial halo. Since $R_{\text{vir}} \sim (M_{\text{vir}})^{1/3}$ this suggests that for fixed D , galaxy mass plays a central role in governing the quantity of MgII absorbing gas. That is, for a sample of galaxies with different masses probed at fixed D , we should see an anti-correlation such that $\log W_r(2796) \sim (-1/3) \log M_{\text{vir}}$. However, the observed scatter with D/R_{vir} and the fact that samples probe a large distribution of D would likely result in "washing out" this relation.

Luminosity Functions

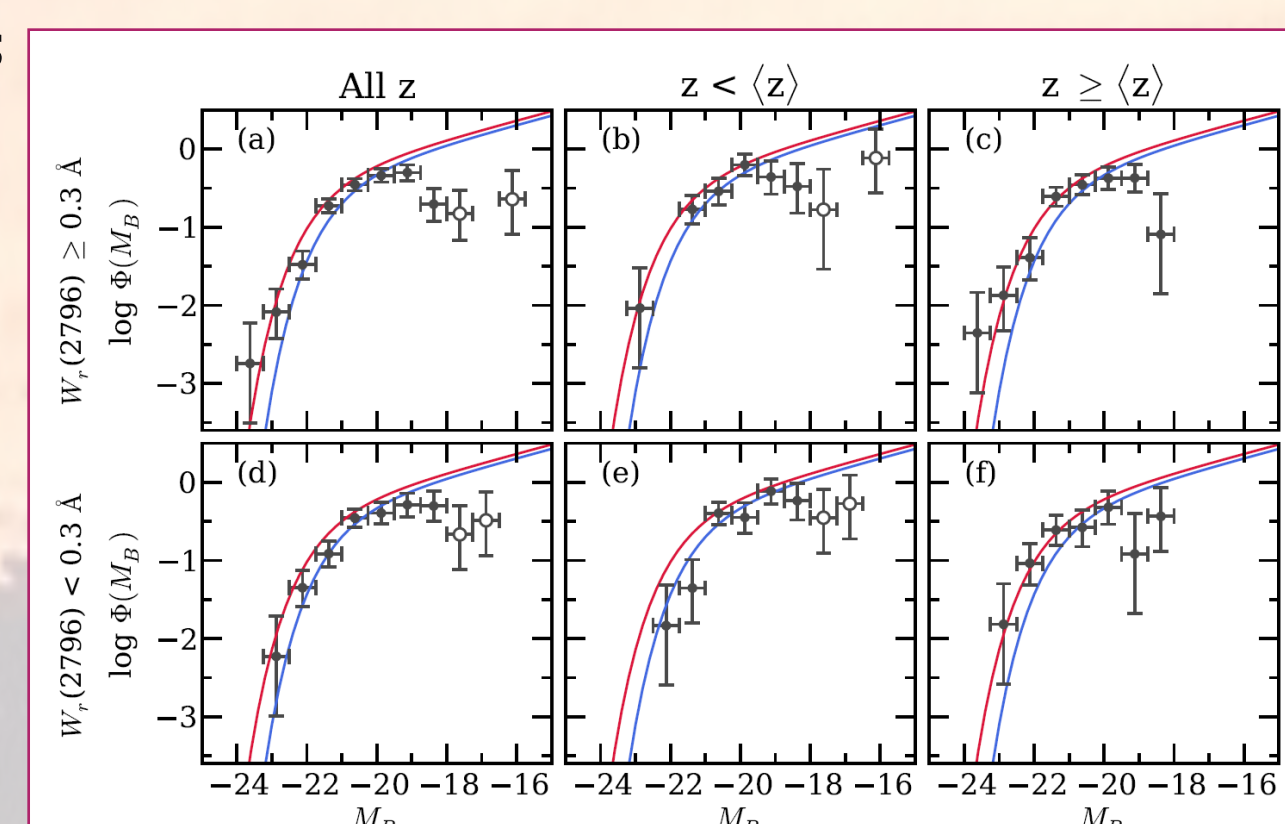
We present the B- and K-band luminosity functions. To determine $\Phi(M)$, we applied a $1/R^2$ area-weighted correction factor, where $R = R_*(L/L_*)^\beta$, to our binned data using $\beta = 0.3$ for the B-band (see Figures 7, 8), and $\beta = 0.3$ for the K-band (data not shown).

In Figure 5, we present $\Phi(M_B)$ for all redshifts (a, d), $z < 0.35$ (b, e), and $z \geq 0.35$ (c, f), bifurcating the sample at $W_r(2796) = 0.3 \text{ \AA}$. In Figure 6, we present $\Phi(M_K)$ for the same subsamples.

Down to $M_B = -18$, we do not confirm the dramatic faint-end turnover in $\Phi(M_B)$ below $M_B = -20.5$ reported by Steidel, Dickinson, & Persson (1994). There may be a turnover below $M_B = -19$ for $W_r(2796) \geq 0.3 \text{ \AA}$, though there is some ambiguity due to the abundance of galaxies below our completeness levels.

Figure 5: $\Phi(M_B)$

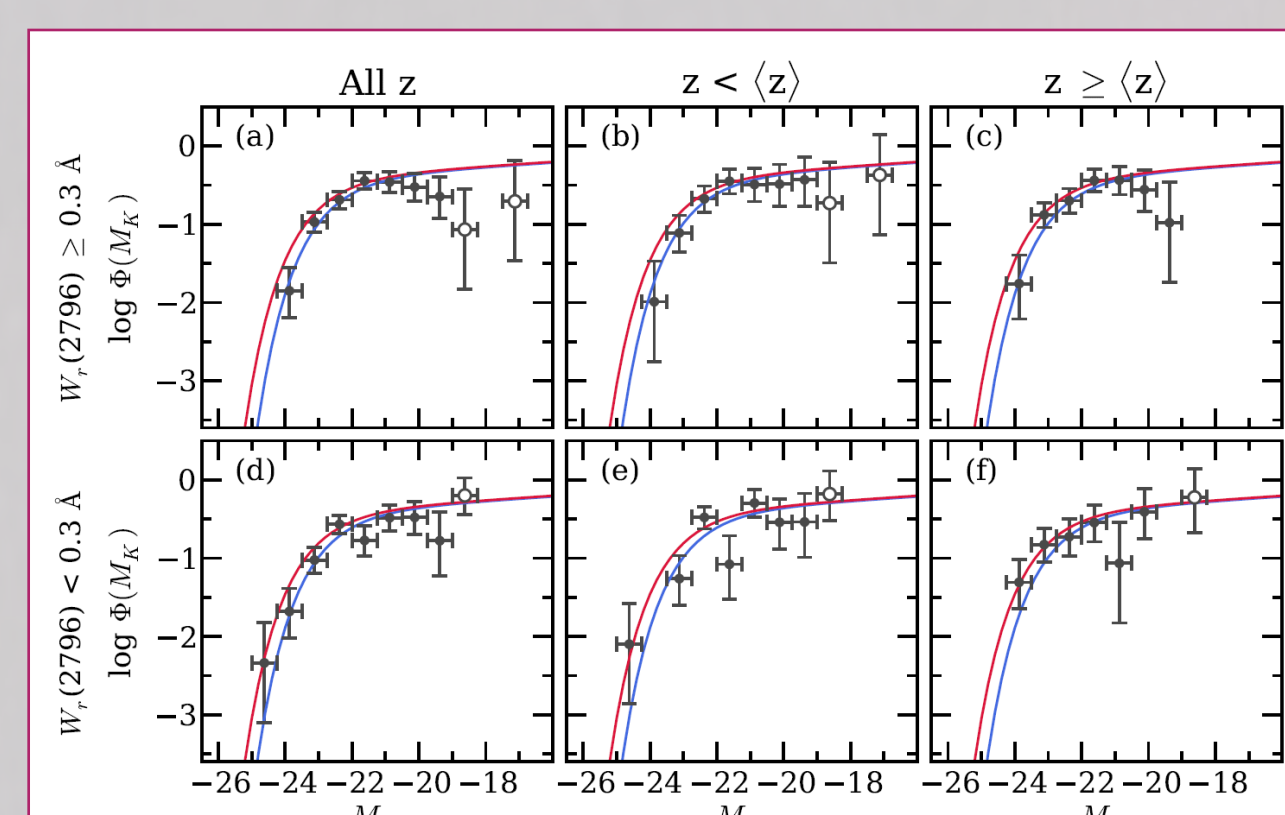
Blue and red curves are $z = 0.3, 1.1$ Schechter functions from Faber et al. 2007. Open points are where the completeness of our sample falls off ($M_B \sim -18$).



For $\Phi(M_K)$, the data are consistent with Cirasuolo et al. (2010) except there may be a cutoff at the bright end at $M_K = -24.5$ for $z \geq 0.35$. For $M_K > -20$ at $z \geq 0.35$, $\Phi(M_K)$ may turnover.

Figure 6: $\Phi(M_K)$

Blue and red curves are $z = 0.3, 1.1$ Schechter functions from Cirasuolo et al. 2010. Open points are where the completeness of our sample falls off ($M_K \sim -19$).



Luminosity Scaling & Covering Fractions

The outer boundary of absorbing gas is commonly assumed to follow a Holmberg-like relation, $R(L) = R_*(L/L_*)^\beta$. We examined whether the B- and K-band halo gas radius also depends on $W_r(2796)$. We apply four $W_r(2796)$ cuts and obtained R_* and β by maximizing the number of galaxies with $W_r(2796) \geq W_{\text{cut}}$ below the fitted line and maximizing the number of galaxies with $W_r(2796) < W_{\text{cut}}$ above the fitted line. In Figure 7, B-band results are presented. The scaling with L_B steepens from $\beta \sim 0.3$ to 0.4 at $W_{\text{cut}} = 0.6 \text{ \AA}$, where $R_* \sim 70 \text{ kpc}$, possibly decreasing for $W_{\text{cut}} = 1 \text{ \AA}$. The covering fraction decreases from 0.94 to 0.39 with increasing W_{cut} . For the K-band, β flattens from 0.3 to 0.1 and R_* decreases from 80 kpc to 55 kpc at $W_{\text{cut}} = 0.6 \text{ \AA}$. The covering fraction decreases from 0.90 to 0.33 with increasing W_{cut} . The K-band data are not shown.

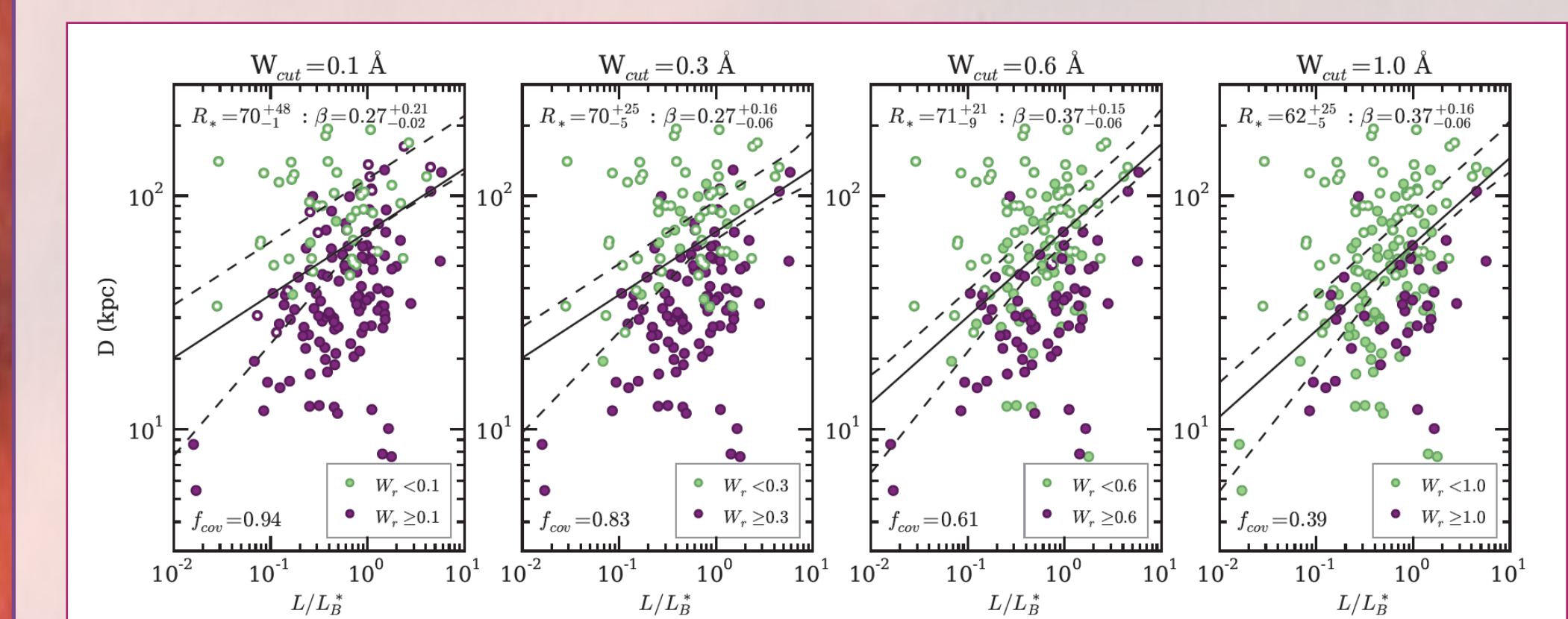
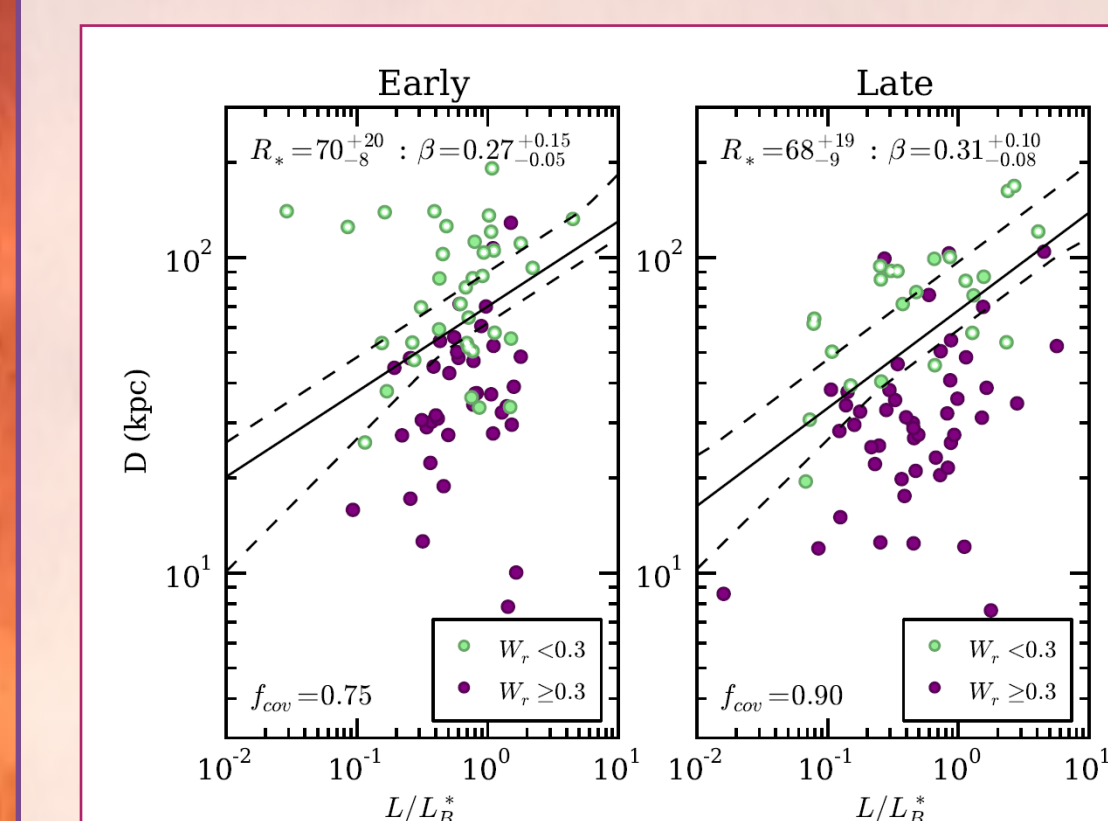


Figure 7: D vs L_B for Different $W_r(2796)$ Bifurcations

In each panel, purple points are galaxies that have a measured $W_r(2796) < W_{\text{cut}}$ and green points are galaxies with $W_r(2796) \geq W_{\text{cut}}$. Open points represent galaxies which have limits on $W_r(2796)$. The fit parameters, R_* , β , and f_{cov} are given for each bifurcation. Dashed lines provide the 1σ uncertainties in the fit.

For the B-band, we compare R_* , β , and f_{cov} between early and late type galaxies for $W_{\text{cut}} = 0.3 \text{ \AA}$, which we illustrate in Figure 8.



The values of R_* and β do not depend on galaxy color (or type), though late types may have a slightly larger covering fraction.

Figure 8: D vs L_B for Early and Late Type Galaxies
Open points represent galaxies which have limits on $W_r(2796)$.

Conclusions

- The sample exhibits no redshift evolution of galaxy color.
- $W_r(2796)$ is anti-correlated with D at the 8.2σ level and is best described as a log-linear relationship down to $W_r(2796) = 0.035 \text{ \AA}$.
- $W_r(2796)$ is anti-correlated with D/R_{vir} at the 9.4σ level and indicates a tight inverse square dependence of $W_r(2796)$ with the projected distance from the galaxy relative to the extent of its virial halo.
- Luminosity functions $\Phi(M_B)$ and $\Phi(M_K)$ appear to be consistent with photometrically selected field galaxies. We do not find the faint-end turnover in $\Phi(M_B)$ reported by Steidel, Dickinson, & Persson (1994).
- The scaling with L_B steepens from $\beta \sim 0.3$ to 0.4 at $W_{\text{cut}} = 0.6 \text{ \AA}$, where $R_* \sim 70 \text{ kpc}$, possibly decreasing for $W_{\text{cut}} = 1 \text{ \AA}$. The covering fraction decreases from 0.94 to 0.39 with increasing W_{cut} .
- The values of R_* and β do not depend on galaxy color (or type), though late types may have a slightly larger covering fraction.

References

- Bryan, G. L., & Norman, M. L. 1998, *ApJ*, 495, 80
 Cirasuolo, M., McLure, R. J., Dunlop, J. S., Almaini, O., Foucaud, S., & Simpson, C. 2010, *MNRAS*, 401, 1166
 Faber, S. M., et al. 2007, *ApJ*, 665, 265
 Kacprzak, G. G., Churchill, C. W., Nielsen, N. M. 2012, *ApJ*, submitted
 Kim, S., Goobar, A., & Perlmutter, S. 1996, *PASP*, 108, 190
 Mannucci, F., Basile, F., Poggianti, B. M., Cimatti, A., Daddi, E., Pozzetti, L., & Vanzli, L. 2001, *MNRAS*, 326, 745
 Ménard, B., et al. 2011, *MNRAS*, 417, 801M
 Rubin, K. H., Prochaska, J. X., Koo, D. C., & Phillips, A. C. 2012, *ApJ*, 747L, 26R
 Trujillo-Gomez, S., Klypin, A., Primack, J., & Romanowsky, A. J. 2011, *ApJ*, 742, 16
 Weiner, B. J., et al. 2009, *ApJ*, 692, 187W
- The following papers were included in our literature search:
 Chen, H.-W., Helsby, J. E., Gauthier, J.-R., Shectman, S. A., Thompson, I. B., & Tinker, J. L. 2010a, *ApJ*, 714, 1521
 Chen, H.-W., & Tinker, J. L. 2008, *ApJ*, 687, 745
 Churchill, C. W., Kacprzak, G. G., Nielsen, N. M., Steidel, C. C., & Murphy, M. T. 2011, *ApJ*, submitted
 Guillemin, P., & Bergeron, J. 1997, *A&A*, 328, 499
 Kacprzak, G. G., Churchill, C. W., Barton, E. J., & Cooke, J. 2011, *ApJ*, 733, 105
 Kacprzak, G. G., Churchill, C. W., Evans, J. L., Murphy, M. T., & Steidel, C. C. 2011, *MNRAS*, 416, 3118
 Kacprzak, G. G., Murphy, M. T., Churchill, C. W. 2010, *MNRAS*, 406, 445
 Steidel, C. C., Dickinson, M., Meyer, D. M., Adelberger, K. L., & Sembach, K. R. 1997, *ApJ*, 480, 568
 Steidel, C. C., Dickinson, M., & Persson, S. E. 1994, *ApJ*, 437, L75